PROJECT 2:
STUDY OF COSMIC CHARGED PARTICLE EVENTS WITH THE POLARQUEEEST EXPERIMENT
FYS5555 - SPRING 2020

ELISABETH CHRISTENSEN

1.1 COSMIC RAYS

The study of cosmic rays began in the beginning of the 20'th century, and was triggered by the fact that radiation was able to penetrate even those of the most isolating materials. Using electrometers, one could measure the intensity of radiation at different altitudes. In 1912, Victor Hess discovered [1] that the radiation increased with increasing altitudes, meaning that the radiation must originate beyond our atmosphere. He excluded the Sun as the sole source of this type of radiation, and concluded that it can also come from more distant sources such as other galaxies. Now, the reason as to why we wish to know more about these cosmic rays is due to their astonishingly high energies. An example of this is the 'Oh-My-God' particle, measured by the Fly's Eye experiment [2], which reached the Earth's surface with an energy of $3.2 \cdot 10^{20}$eV, i.e. more than a billion times greater than what our most advanced accelerators to date can manage. This leaves us with the bigger questions to answer. Where do these particles come from and how did they reach such high energies?

Primary cosmic rays are essentially high-energetic protons and alpha particles originating from the Sun or beyond our Solar system. Models indicate that cosmic rays of energies up to $\sim 10^{15}$eV originate from the shock fronts of supernova remnants [3]. The AGASA observatory, situated in Japan, measures the higher end of the energy spectrum, i.e. up to 10^{20}eV, of cosmic rays entering our atmosphere. Another observatory, the Pierre Auger Observatory, published its first results of the highest-energy cosmic rays in 2007. The observatory has also assisted in finding the energy spectrum for cosmic rays above $\sim 10^{18}$eV [4], and found that the flux was propotional to $E^{-\gamma}$, where γ is approximately equal to 3. It also supported the theory that within the center of each galaxy resides a black hole with the capacity to accelerate particles to energies up to 10^{20}eV.

Secondary cosmic rays are essentially particle showers occuring when the primary cosmic rays interact with particles within our atmosphere. These cosmic rays typically consist of neutrons and charged mesons which subsequently can decay to muons and neutrinos reaching the Earth's surface.

There are many experiments dedicated to use secondary cosmic particles in the search for knowledge. Some examples are the CLOUD experiment at CERN [5], designed to measure the correlation between cosmic rays and cloud formation, the balloon-borne experiment TRACER [6] designed to observe cosmic-ray nuclei at high energies, and the ground-based Cherenkov Telescope Array (CTA) observatory [7], dedicated to find the origin and role of relativistiv cosmic particles through the study of high-energy gamma-rays reaching Earth.

2.1 POLA DETECTORS

Particles can be detected in numerous ways depending on their charge and energy, some examples being the ionization chamber, the proportional counter and the Geiger-Müller counter. The Geiger-Müller counter was one of the first few devices to detect particles and consists simply of an air-tight cylinder tube containing a suitable gas and a suspended conducting wire with a positive voltage. When charged particles strike the gas they interact with molecules within the gas creating electron-ion pairs. The electrons will be accelerated towards the conducting wire, i.e. the anode, whereas ions will be accelerated towards the cathode. The total eletron-ion pairs collected results in a measurable electric current. Another example is that of scintillators.

Scintillators are based on the principle of luminescense [8]. In other words, as passing radiation strikes a luminescent material it converts the kinetic energy of the charged particles to detectable light. Put simply, scintillators gather the information of the emitted photons in photomultiplier tubes which outputs a current of electrons based on the energy of the impinging photon.

Each of the POLA detectors consists of two floors of four plastic scintillators with the dimensions $20 \times 30 \times 1 \mathrm{cm}^3$. The main purpose of a plastic scintillator is to emit photons within the energy range of any passing charged particle. Plastic scintillators can provide an extremely fast signal with a decay constant of about 2-3ns along with a high light output [9]. Attached to each scintillator is a pair of silicon photomultiplier (SiPM) tubes. Included are also eight front-end boards each dedicated to handle the SiPM signals separately, and trigger on events with a 10ns resolution.

3.1 ENVIRONMENTAL CONDITIONS

From figure 1a we can see the variations in indoor temperature onboard the 18m long sailboat Nanuq containing the detector POLA-01, from 22'nd of July 2018 to 4'th of September 2018. Each point represents the average indoor temperature recorded per event over a time interval of 10 minutes. The corresponding indoor temperatures for POLA-02 and POLA-03 can be seen in figures 1b and 1c. Figure 2 shows the temperatures close to the electronics for each detector. The corresponding mean values and sample

TABLE 1. Mean values of indoor, $\mu_{T,in}$, and outdoor, $\mu_{T,out}$, temperatures of each detector.

	$\mu_{T,in}(^\circ\mathrm{C})$	$\mu_{T,out}(^\circ\mathrm{C})$
POLA-01	25.39 ± 2.79	23.75 ± 2.73
POLA-02	25.06 ± 0.14	24.13 ± 0.12
POLA-03	33.37 ± 0.85	34.67 ± 0.75

TABLE 2. Pressure as measured by each detector.

	μ_P
POLA-01	1012.62 ± 8.68
POLA-02	1008.56 ± 6.55
POLA-03	985.96 ± 2.63

standard deviations of the temperatures can be seen in table 1. Here, we see that the variations in temperature for POLA-01 are much greater than that for POLA-02 and POLA-03, which can be explained by the fact that it was subject to varying weather conditions while travelling between Isafjord, Iceland and Tromsø, Norway.

Figure 3 shows the atmospheric pressure each detector is subject to. This is dependent on the surrounding temperature and the elevation above sea level. As can be seen for POLA-03, situated in Bra, Italy, the pressure remains lower due to its elevation of approximately 278m above sea level. The effects of elevation can also be seen for POLA-02, situated in Nesodden, Norway at 81m, and POLA-01 onboard the sailboat Nanuq, which are subjects to a higher overall atmospheric pressure than that of POLA-03. The fluctuations of the atmospheric pressure arises due to the variations in temperature. One can see that the pressure resembles the patterns of temperature in figures 1 and 2.

3.2 PARTICLE RAW RATE

The particle raw rate can be seen in figure 4. Here, each point corresponds to a measurement of the number of events divided by time at every 12 hours. The raw rate is dependent on the atmospheric pressure, i.e. when the pressure drops there is a lower absorption of particles, thus resulting in a higher rate. The rate is also dependent on the materials surrounding the detectors. This can also be the reason why POLA-03 shows a lower raw rate compared to POLA-01 and POLA-02, because it may be surrounded by more dense materials, or be in a more compact room.

3.2.1 LONGITUDE AND LATITUDE

The latitude and longitude for POLA-01 onboard Nanuq can be seen in figure 5. We see from figure 4 that the rate is relatively flat, which is to be expected from the theory of Arthur Compton from 1933, in which the intensity of cosmic rays remains constant approximately above latitudes of

Indoor temperature POLA-01
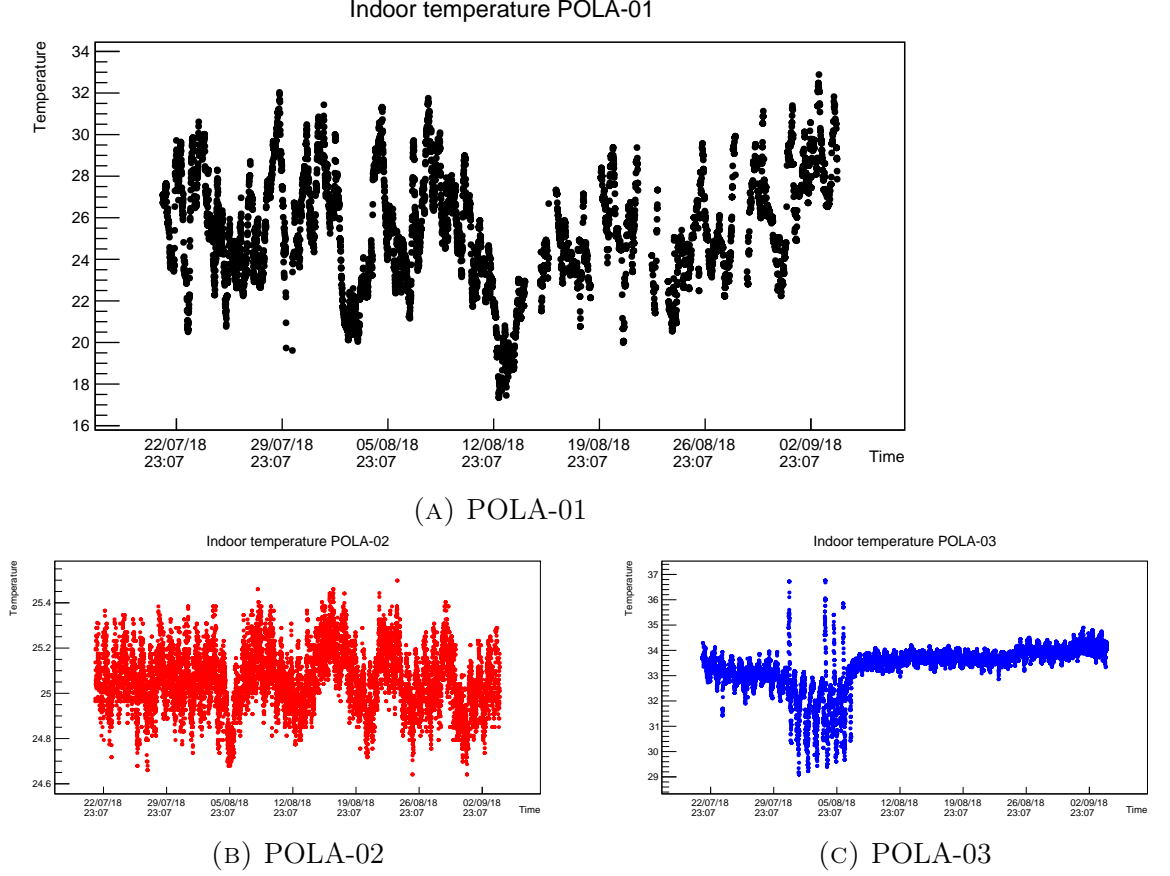

(A) POLA-01

(B) POLA-02

(C) POLA-03

FIGURE 1. Indoor temperature as measured within each room containing the detectors.

60°N. When compared to the POLA-02 as a reference point, the variations[1] of the raw rate is 2.04%.

3.2.2 PRESSURE AND TEMPERATURE

The raw rate as a function of the pressure can be seen in figure 6a. Here, we see a clear distinction between the detectors. The POLA-01 and POLA-02 detectors are each subject to approximately the same pressure in which the raw rate appears to be higher than POLA-03. However, as explained above, this may be due to the materials the detector POLA-03 was surrounded by. We see however a negative gradient of the rate in all three detectors as the pressure increases, as expected. In figure 6b we see that the rate remains approximately constant, i.e. independent of the temperature. The gradients of the raw rate as a function of pressure and temperature for each detector was found by linear regression and can

---

[1]This is performed for the raw rates of POLA-01 and POLA-02, i.e. $\sigma\left(\frac{POLA-01/\langle POLA-01\rangle}{POLA-02/\langle POLA-02\rangle}\right)$, in which we have excluded the two outliers of figure cor-responding to values less than 10.

(A) POLA-01

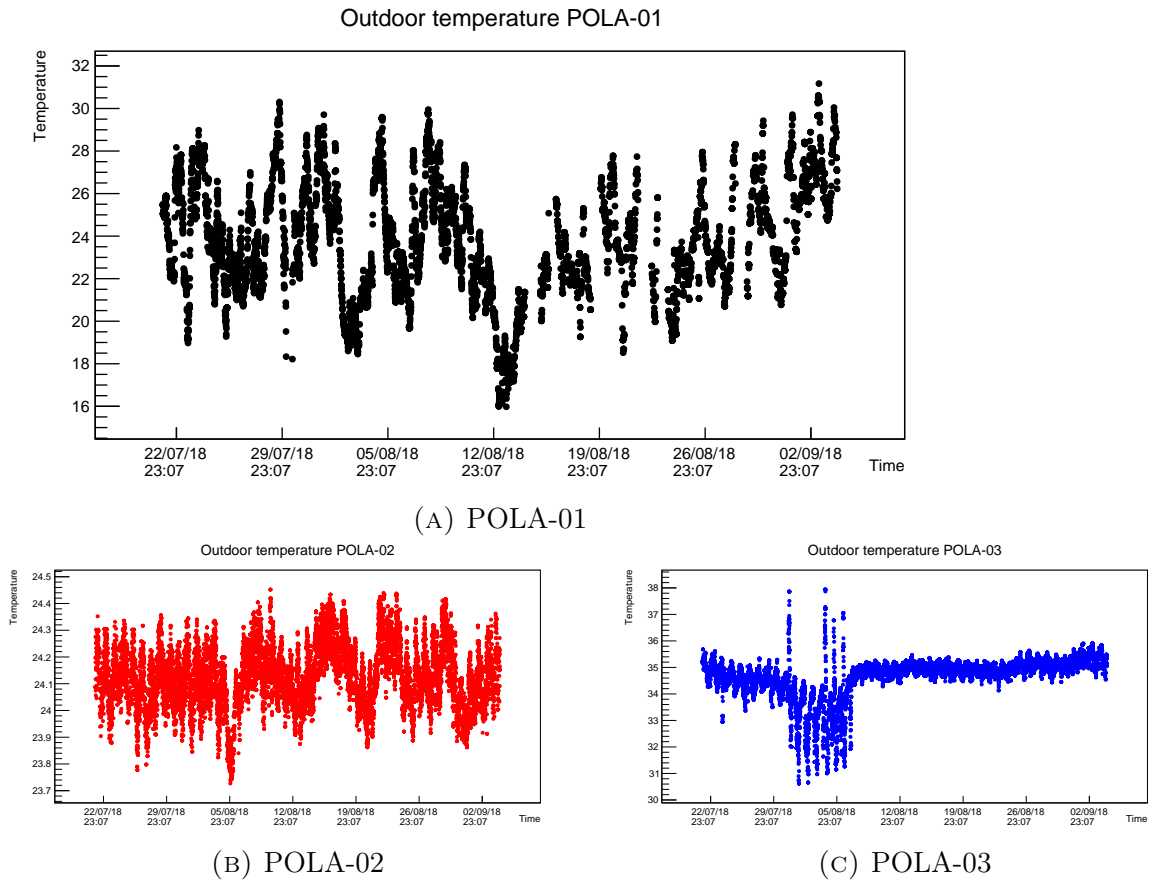
(B) POLA-02

(C) POLA-03

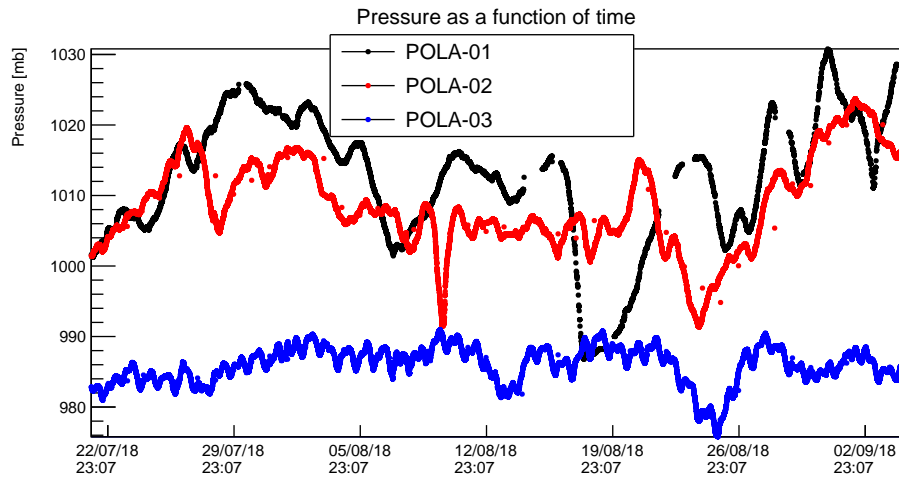FIGURE 2. Outdoor temperature as measured close to the electronics of each detector.

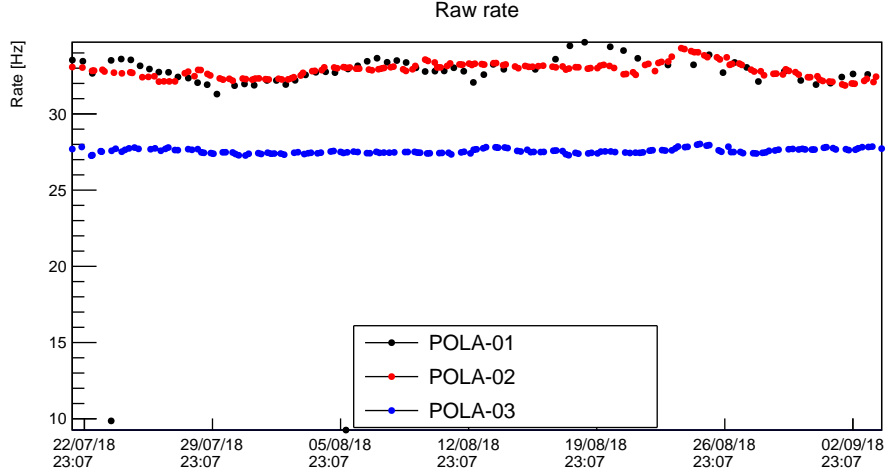FIGURE 3. Barometric pressure each detector is subject to dependent on elevation above sea level.
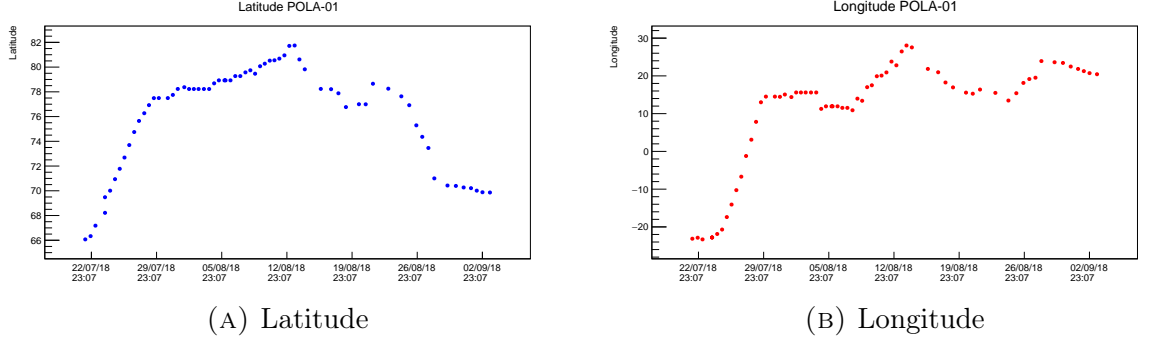
FIGURE 4. Raw rate as measured by each detector.

(A) Latitude   (B) Longitude

FIGURE 5. Latitude and longitude of POLA-01 measured at every 12 hours.

TABLE 3. Gradients of the raw rate as a function of pressure, P, and outdoor temperature, T_{out}.

	P	T_{out}
POLA-01	-7.047e-02	-4.307e-03
POLA-02	-6.808e-02	0.533
POLA-03	-4.127e-02	0.0610

be seen in table 3. Here[2], the gradients of the raw rate as a function of the pressure P are relatively consistent with one another confirming the statement above. However, when looking at the rate as a function of the temperature then the gradients do not appear as consistent, which may be due to lack of data included in the linear regression thus causing greater uncertainties.

---

[2]The raw rate for POLA-01 has been corrected by excluding the two outliers as seen in figure 4.
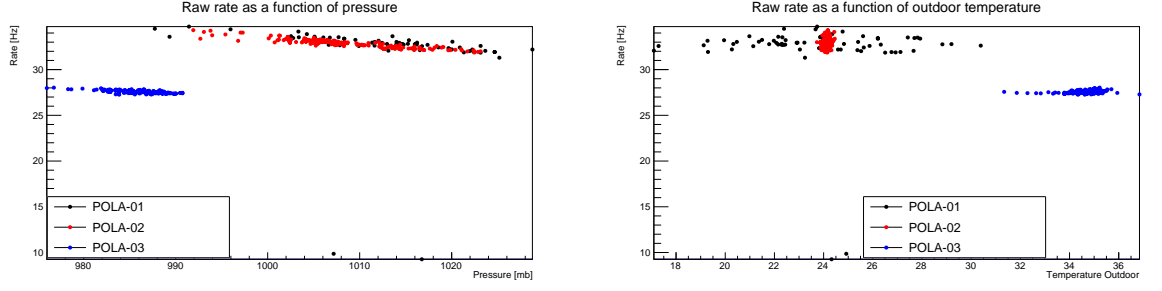
(A) Raw rate as function of pressure.

(B) Raw rate as function of temperature.

FIGURE 6. Raw rate as function pressure and of the outdoor temperature close to the electronics.

TABLE 4. Values for parameters α and β for the barometric correction coefficients as found by linear regression.

	α	β
POLA-01	3.457	-1.795e-03
POLA-02	3.493	-2.069e-03
POLA-03	3.317	-1.493e-03

3.2.3 CORRECTED RAW RATE

The barometric correction coefficients, $\gamma(p)$, to the raw rate can be expressed as

$$\gamma(p) = e^{\alpha + \beta(p - p_{ref})} \tag{1}$$

where α and β can be found by a least squares polynomial fit to the first degree. In doing so we find the values as shown in table 4.

In calculating the corrected rate we can divide the raw rate by the barometric corrected coefficients, in which we choose to ignore α. This is due to the fact that α can still be considered a biased parameter dependent on the conditions as discussed above. The corrected rate over time can be seen in figure 7 which, compared to figure 4, displays smoother curves resulting in less variance in our dataset. The mean values of the raw and corrected rates can be seen in table 5[3]. As a final note, the rate for the POLA-03 detector, as explained above, lies systematically lower than that of POLA-01, and POLA-02, which can be caused by how dense the material surrounding the detectotr is. Thus, the materials surrounding a detector can have a significant effect on the rate measured.

REFERENCES

[1]V. Hess, "On the observations of the penetrating radiation during seven balloon flights", (1912).

---

[3]Note however that the variance for the POLA-01 detector is nearly unchanged. This may be due to the two outliers of the rates as can be seen in figures 4 and 7, with values below 10Hz.

TABLE 5. Comparison of the raw and corrected rates for each detector.

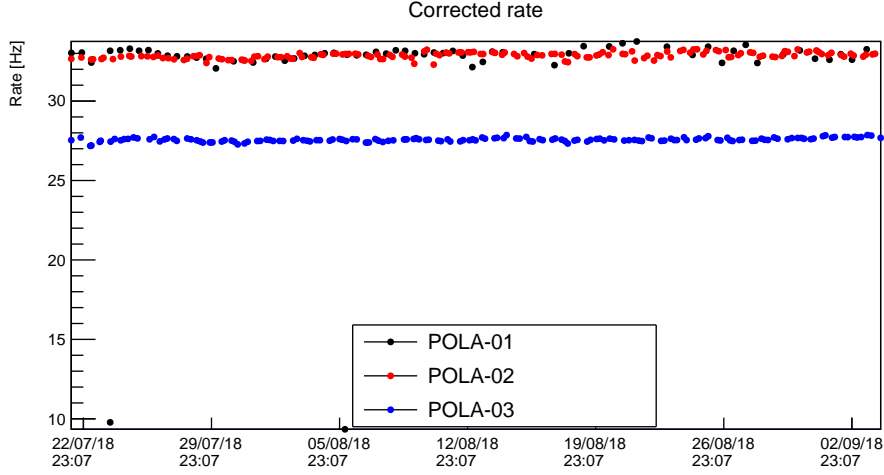|	Raw	Corrected
POLA-01	32.18 ± 4.09	32.22 ± 4.05
POLA-02	32.87 ± 0.49	32.87 ± 0.19
POLA-03	27.56 ± 0.16	27.57 ± 0.11

FIGURE 7. Corrected raw rate as a function of time.

[2]D. J. Bird, S. C. Corbato, H. Y. Dai, J. W. Elbert, K. D. Green, M. A. Huang, D. B. Kieda, S. Ko, C. G. Larsen, E. C. Loh, and et al., "Detection of a cosmic ray with measured energy well beyond the expected spectral cutoff due to cosmic microwave radiation", The Astrophysical Journal **441**, 144 (1995).

[3]D. C. Ellison, L. O. Drury, and J.-P. Meyer, "Galactic cosmic rays from supernova remnants. II. shock acceleration of gas and dust", The Astrophysical Journal **487**, 197–217 (1997).

[4]G. Matthiae, "The cosmic ray energy spectrum as measured using the pierre auger observatory", New Journal of Physics **12**, 075009 (2010).

[5]F. B. et al, "Cloud: an atmospheric research facility at cern", (2000).

[6]D. Müller, M. Ave, P. Boyle, F. Gahbauer, C. Höppner, A. Romero-Wolf, J. Hörandel, and M. Ichimura, "Proceedings, 30th International Cosmic Ray Conference (ICRC 2007): Merida, Yucatan, Mexico, July 3-11, 2007", **2**, 83–86 (2007).

[7]M. Actis, G. Agnetta, F. Aharonian, and et al., "Design concepts for the cherenkov telescope array cta: an advanced facility for ground-based high-energy gamma-ray astronomy", Exp Astron 32 (2011).

[8]G. F. Knoll, *Radiation detection and measurement*, Vol. 3 (John Wiley & Sons, Inc., 2000), pp. 219–247.

[9]W. R. Leo, *Techniques for nuclear and particle physics experiments, a how-to approach*, Vol. 2 (Springer-Verlag Berlin Heidelberg, 1994), pp. 159–164.